Synthesis, structural analysis, Hirshfeld surface analysis, DFT calculations, in vitro and docking study on antioxidant activity of 6-chloro-3-[(4-methylphenoxy) methyl] [1,2,4] tr...

Article · September 2021

DOI: 10.1080/15421406.2021.1907053

CITATIONS
0

READ
1

5 authors, including:

Hamdi Hamid Sallam
University of Mysore
4 PUBLICATIONS **7** CITATIONS
SEE PROFILE

Geetha D. V.
University of Mysore
9 PUBLICATIONS **43** CITATIONS
SEE PROFILE

Fares Hezam Al-Ostoot
University of Mysore
46 PUBLICATIONS **150** CITATIONS
SEE PROFILE

Molecular Crystals and Liquid Crystals

ISSN: (Print) (Online) Journal homepage: https://www.tandfonline.com/loi/gmcl20

Synthesis, structural analysis, Hirshfeld surface analysis, DFT calculations, *in vitro* and docking study on antioxidant activity of 6-chloro-3-[(4-methylphenoxy) methyl] [1,2,4] triazolo[4,3-b]pyridazine

Hamdi Hamid Sallam, Yasser Hussien Eissa Mohammed, Geetha D. V., Fares Hezam Al-Ostoot, Sridhar M. A. & Ara Khanum Shaukath

To cite this article: Hamdi Hamid Sallam, Yasser Hussien Eissa Mohammed, Geetha D. V., Fares Hezam Al-Ostoot, Sridhar M. A. & Ara Khanum Shaukath (2021): Synthesis, structural analysis, Hirshfeld surface analysis, DFT calculations, *in vitro* and docking study on antioxidant activity of 6-chloro-3-[(4-methylphenoxy) methyl] [1,2,4] triazolo[4,3-b]pyridazine, Molecular Crystals and Liquid Crystals, DOI: 10.1080/15421406.2021.1907053

To link to this article: https://doi.org/10.1080/15421406.2021.1907053

Published online: 17 Sep 2021.

MOLECULAR CRYSTALS AND LIQUID CRYSTALS
https://doi.org/10.1080/15421406.2021.1907053

Synthesis, structural analysis, Hirshfeld surface analysis, DFT calculations, *in vitro* and docking study on antioxidant activity of 6-chloro-3-[(4-methylphenoxy) methyl] [1,2,4] triazolo[4,3-b]pyridazine

Hamdi Hamid Sallam[a,b], Yasser Hussien Eissa Mohammed[c,d], Geetha D. V.[a], Fares Hezam Al-Ostoot[c,e], Sridhar M. A.[a], and Ara Khanum Shaukath[c]

[a]Department of Studies in Physics, Manasagangotri, University of Mysore, Mysuru, India; [b]Department of Physics, Faculty of Education and Science, Turba Branch, Taiz University, Taiz, Yemen; [c]Department of Chemistry, Yuvaraja's College, University of Mysore, Mysuru, India; [d]Department of Biochemistry, Faculty of Applied Science, University of Hajjah, Hajjah, Yemen; [e]Department of Biochemistry, Faculty of Education and Science, Al-Baydha University, Al-Baydha, Yemen

ABSTRACT

Pyridazine nuclei are essential elements of many natural and synthetic compounds with important biological activities. NMR and IR, as well as studies of mass spectrum, were emplyed to synthesize and characterize the title compound 6-chloro-3-[(4-methylphenoxy) methyl] [1,2,4] triazolo[4,3-b] pyridazine (CMTP). The structure of this compound was confirmed by using single crystal X-ray diffraction technique and it got crystallized in the monoclinic crystal system with the space group $P2_1/c$. The values of unit cell parameters are: $a = 12.0965(7)$ Å, $b = 13.6075(7)$ Å, $c = 7.7686(4)$ Å, $\beta = 93.942(3)^\circ$ and $Z = 4$. Intermolecular hydrogen bonds of two types i.e., C-H … O and C-H … N, were noticed. Hirshfeld surface analysis was employed to account for these interaction bonds. Energy frameworks were carried out to know the dominant interaction energy involved in the molecular packing. DFT calculations were constructed to find the agreement between the theoretical and experimental values. HOMO-LUMO energy levels have been determined; global hardness, global softness, and other quantum chemical parameters have been calculated to reveal the chemical reactivity of the compound. In order to investigate the antioxidant activity of the compound, molecular docking studies were performed.

KEYWORDS

Pyridazines; XRD and DFT calculations; Hirshfeld surface; energy framework; antioxidant activity; docking study

1. Introduction

Heterocyclic aromatic compounds are the most important sources for synthesizing novel compounds that have a significant interest as a result of their unique properties and amazing effects [1]. Nitrogen containing heterocycles compounds show diverse biological properties [2]. Pyridazine is an aromatic ring having two adjacent nitrogen atoms. Multiple nitrogen atoms in these compounds present unique chemistry [3]. The pyridazine-derived compounds show antibacterial, antifungal, and antiviral activities [4].

CONTACT Sridhar M. A. mas@physics.uni-mysore.ac.in Department of Studies in Physics, Manasagangotri, University of Mysore, Mysuru 570 006, India.

The pyridazine nucleus represents a versatile scaffold to develop new pharmacologically active compounds [5, 6] which can act as potential anti-microbial, anti-hypertensive [7], anti-cancer [8], anti-inflammatory [8, 9], anti-HAV [10] and anti-fungal agents [11]. Pyridazine with other heterocyclic/pharmacophoral ring possesses potential antitumor activity [12–14]. In view of their broad spectrum of biological properties, and as a part of our ongoing work [15, 16], synthesis and characterization of the title compound are carried out. The compound was characterized by various spectroscopic techniques and the structure was determined by a single crystal X-ray structural analysis, theoretical calculations were also carried out.

2. Materials and methods

2.1. Experimental

The chemicals required for the synthesis of the title compound (CMTP) were procured from Sigma Aldrich Chemical Co. The progress of the reaction was monitored by thin layer chromatography (TLC) performed on aluminium-backed silica plates, and the spots were detected by exposure to UV-lamp at $\lambda = 254$ nm. Melting point and boiling point were measured on a Chemiline, microcontroller based melting point/boiling point-Cl725 apparatus with a digital thermometer. IR spectra were recorded on the Agilent Technologies Cary 630 FTIR spectrometer. ^{1}H and ^{13}C NMR spectra were recorded on VNMRS-400 Agilent-NMR spectrophotometer. The mass spectra were obtained with a VG70-70H spectrometer. The elemental analysis (C, H, and N) was performed on Elementar Vario EL III elemental analyzer. The result of elemental analysis is within ±0.4% of the theoretical value.

2.1.1. Synthetic procedure for ethyl 2-(4-tolyloxy)acetate (3)

To a solution of substituted phenol (**1**, 0.03 mol) in dry acetone (35 ml), anhydrous potassium carbonate (6.4 g, 0.044 mol) and ethyl chloroacetate (2, 0.044 mol) were added. The reaction mixture was refluxed at 70 °C for 10 h to afford phenoxyacetic ethyl ester (**3**). The progress of the reaction was monitored by TLC [mobile phase: ethyl acetate/hexane (1:3)]. After completion of the reaction, the mixture was cooled and the solvent was removed by distillation. The residual mass was triturated with cold water to remove potassium carbonate and extracted with ether (3 × 30 ml). The ether layer was washed with 10% sodium hydroxide solution (3 × 30 ml) followed by water (3 × 30 ml) and then dried over anhydrous sodium sulfate and evaporated to afford compound (**3**) as yellow liquid which slowly solidifies [17].

2.1.2. Synthetic procedure for 2-(p-tolyloxy)acetic acid (4)

The phenoxy ester (**3**, 0.02 mol) was dissolved in ethanol (12 ml), 35% sodium hydroxide solution (2 ml) was added and the mixture was refluxed for 5–9 h. The reaction was monitored by TLC using hexane: ethyl acetate: methanol (6:3:1). The reaction mixture was cooled and quenched with 2 N hydrochloric acid [8]. The precipitate was filtered, washed with water, and finally recrystallized to afford the compound (**4**).

2.1.3. Synthetic procedure for 3-chloro-6-hydrazinylpyridazine (6)

After stirring the compound (**3**), 6-Dichloropyridazine (2 mmol) in ethanol (25 ml) for 30 min at room temperature, hydrazine hydrate (2 mmol) was added. The reaction was further refluxed for 1 h at 100 °C. It was monitored by TLC using hexane: ethyl acetate (6:2) as the mobile phase. The white product of 3-chloro-6-hydrazinylpyridazine (**6**) was filtered, washed, dried, and recrystallized from ethanol [18].

2.1.4. Synthetic procedure forN′-(6-chloropyridazin-3-yl)-2-(p-tolyloxy)acetohydrazide (7)

To acetic acid (**4**, 2 mmol) stirring in dry DCM (20 ml), lutidine (3 mmol) was added at 25-27 °C, followed by the addition of 3-chloro-6-hydrazinylpyridazine (**6**, 2 mmol). The reaction mixture was stirred at the same temperature for 35 min. After reducing the temperature to 0–5 °C, TBTU (2 mmol) was added to the mixture. The temperature was maintained below 5 °C for a period of 30 min. The reaction mass was stirred overnight and monitored by TLC. The solvent was evaporated under reduced pressure, quenched by the addition of crushed ice, and the solid obtained was filtered and dried. This crude product was subjected to column chromatography, and eluted with the solvent mixture of ethyl acetate: hexane (4:1) to get the pure product which was recrystallized to afford compound (**7**) [8].

2.1.5. Synthetic procedure for chloro-3-((p-tolyloxy)methyl)-[1,2,4]triazolo[4,3-b] pyridazine (CMTP) (8)

The pyridazine phenoxy acetohydrazide (**7**, 0.40 g, 0.02 mol) and chloroamine T (2 mmol) in ethanol were heated and refluxed with stirring for 5 h. Sodium chloride formed in the reaction was filtered off, and washings were evaporated in a vacuum; the residue was extracted with 5% hydrochloric acid, and washed thoroughly with dichloromethane. The aqueous layer was neutralized with 10% sodium hydroxide to give CMTP (**8**) (Fig. 1).

2.2. Spectral data

2.2.1. Ethyl 2-(4-tolyloxy)acetate (3)

Yield 88%; B.P. 141–144 °C; FT-IR (KBr, ν_{max} cm^{-1}): 1731–1760 (ester, C = O), 1127–1259 (ester, C–O); ^{1}H NMR (400 MHz, DMSO) δ (ppm): 1.46 (t, $J = 7$ Hz, 3H, CH_3 of ester), 2.38 (s, 3H, CH_3), 4.55 (q, $J = 6$ Hz, 2H, CH_2 of ester), 5.04 (s, 2H, OCH_2), 6.94 (d, $J = 8.80$ Hz, 2H, Ar-H), 7.09 (d, $J = 8.80$ Hz, 2H, Ar-H); LC-MS *m/z* 195 $[M+1]$. Anal. Calcd for $C_{11}H_{14}O_3$ (194): C, 68.02; H, 7.27. Found: C, 68.01; H, 7.18%.

2.2.2. 2-(p-Tolyloxy)acetic acid (4)

Yield 81%; M.P. 142–144 °C; FT-IR (KBr, ν_{max} cm^{-1}): 1730–1745 (C = O), 1253–1262 (Ar–O-C), 3375–3380 (OH); ^{1}H NMR (400 MHz, DMSO) δ (ppm): 2.39 (s, 3H, CH_3), 4.66 (s, 2H, OCH_2), 6.79–6.84 (d, $J = 8.80$ Hz, 2H, Ar-H), 7.03–7.09 (d, $J = 8.80$ Hz, 2H,

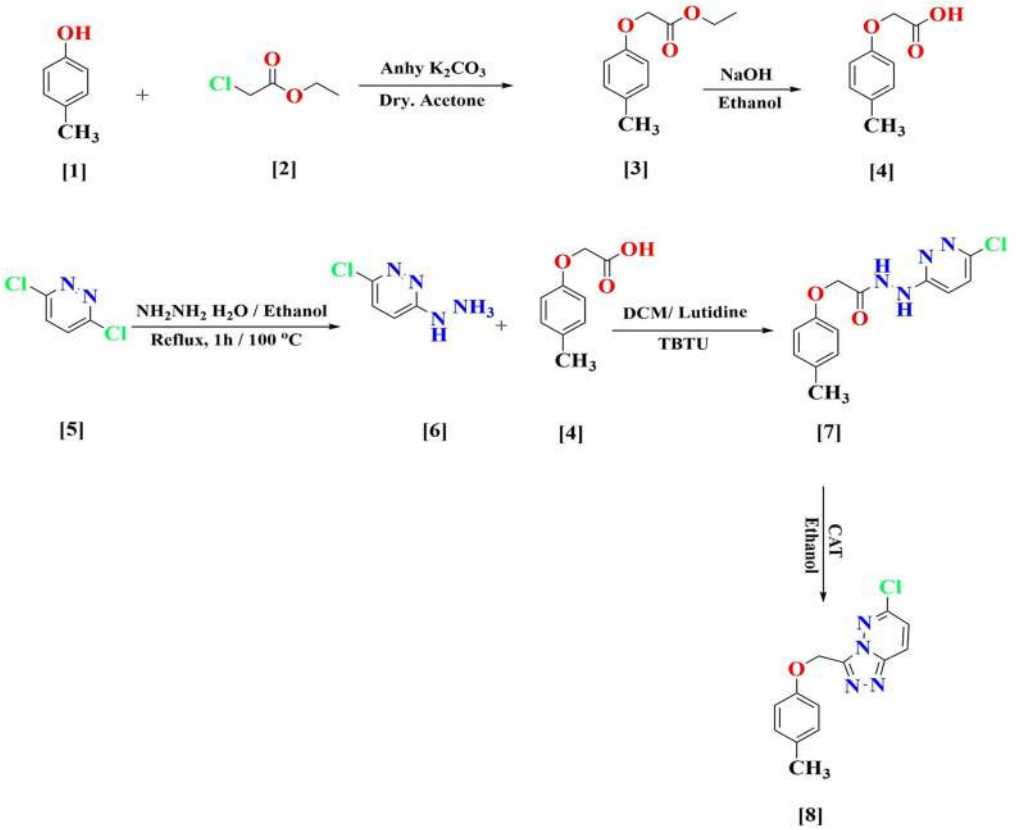

Figure 1. Reaction pathway for the synthesis of the title compound CMTP (**8**).

Ar-H), 13.13 (bs, 1H, OH); LC-MS *m/z* 167 [*M* + 1]. Anal. Calcd. for $C_9H_{10}O_3$ (166): C, 65.05; H, 6.07. Found: C, 65.02; H, 6.04%.

2.2.3. 3-chloro-6-hydrazinylpyridazine (6)

Yield 65%; M.P. 136–138 °C; FT-IR (KBr, ν_{max} cm^{-1}): 1178–1181 (C = N), 3327–3139 (hydrazine $NHNH_2$); ^1H NMR (400 MHz, DMSO) δ (ppm): 4.59 (bs, 2H, NH_2), 7.21 (d, J = 8 Hz, 2H, Ar-H), 8.48 (s, 1H, NH); LC-MS *m/z* 145 [M+] 147 [*M* + 2]. Anal. Calcd. for $C_4H_5ClN_4$ (145): C, 33.23; H, 3.49; N, 38.76. Found: C, 33.21; H, 3.47; N, 38.73%.

2.2.4. N′-(6-chloropyridazin-3-yl)-2-(p-tolyloxy)acetohydrazide (7)

Yield 84%; M.P 127–129 °C; FT-IR (KBr, ν_{max} cm^{-1}): 1675 (C = O), 3124–3230 (NH-NH); ^1H NMR (400 MHz, DMSO) δ (ppm): 2.25 (s, 3H, CH_3), 4.71 (s, 2H, OCH_2), 6.89 (d, J = 9.2 Hz, 2H, Ar-H), 7.05 (d, J = 9.2 Hz, 1H, 4-pyridazin-H), 7.10 (d, J = 9.2 Hz, 2H, Ar-H) 7.20 (d, J = 9.2 Hz, 1H, 5-pyridazin-H), 8.99 (s, 1H, NH), 10.94 (s, 1H, NH); ^{13}C NMR (100 MHz, DMSO): δ 22.91, 67.29, 115.29, 119.87, 129.39, 130.01, 132.17, 152.38, 158.55, 164.06, 168.76; LC-MS *m/z* 293 [M+] 295 [*M* + 2]. Anal. Calcd. For $C_{13}H_{13}ClN_4O_2$ (293): C, 53.34; H, 4.48; N, 19.14. Found: C, 53.32; H, 4.45; N, 19.12%.

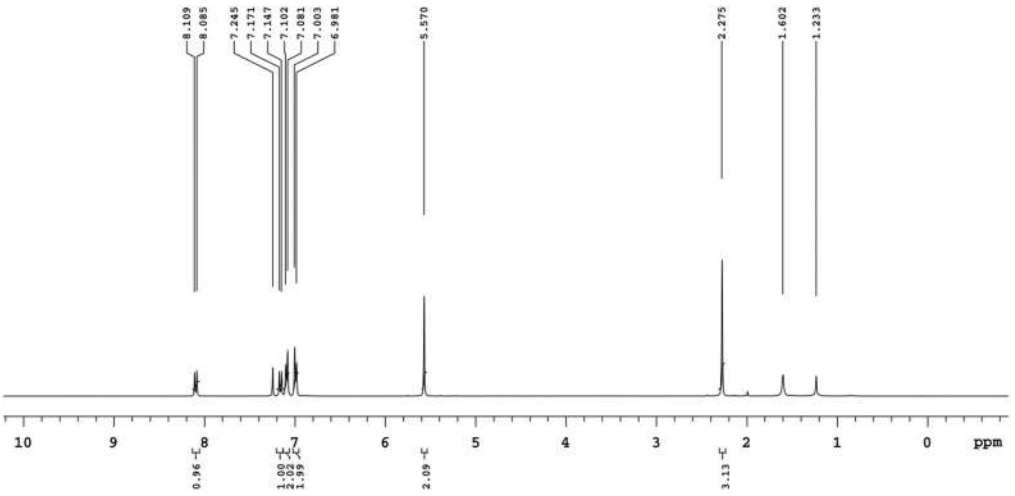

Figure 2. ^{1}HNMR spectrum of the compound CMTP.

2.2.5. Chloro-3-((p-tolyloxy)methyl)-[1,2,4]triazolo[4,3-b] pyridazine (CMTP) (8)

Yield: 82%.M.P 117–121 °C. IR (KBr, ν_{max} cm^{-1}): 1341 (C = N), ^{1}H NMR (400 MHz, DMSO) δ (ppm): 2.27 (s, 3H, CH_3), 5.57 (s, 2H, CH_2), 6.98–8.10 (m, 6H, Ar-H) as shown in Fig. 2. ^{13}C NMR (100 MHz, DMSO) δ (ppm): 21.33, 67.66, 114.23, 123.01, 127.11, 130.12, 132.02, 141.99, 150.01, 156.23, 1632. LC-MS *m/z* 275 ($M+1$), 277 ($M+2$). Anal. Cal. For $C_{13}H_{11}ClN_4O$ (274): C, 56.84; H, 4.04; N, 20.40. found C, 56.88; H, 4.14; N, 20.41%.

2.3. X-Ray intensity data collection, structure solution and refinement

A block of yellow colored single crystal with approximate dimensions $0.20 \times 0.15 \times 0.10\,mm^3$ was chosen for X-ray data collection. The data were collected on a Bruker CMOS diffractometer equipped with MoK_α radiation with wavelength 0.71073 Å at 293 K. The data reduction of all the measured reflections was done using *APEX*3 [19] package. The crystal structure was solved by direct methods using *SHELXS*-97. Using *SHELXL*-97 [20], the refinement against F^2 was carried out. All the non-hydrogen atoms were refined anisotropically. Hydrogen atoms attached to carbon atoms were allowed to ride on their parent atoms. Using *PLATON* [21], geometrical calculations were carried out. The molecular graphics were generated using *MERCURY* [22]. A total of 174 parameters were refined with 2606 unique reflections which converge the residual factor R to 0.053.

Crystallographic data (CIF) of the compound CMTP has been deposited at the Cambridge Crystallographic Data Centre with CCDC No. 1838281. Table 1 lists the crystal data, and refinement details.

3. Results and discussion

3.1. X-Ray diffraction, DFT calculations and frontier molecular orbitals

The title compound ($C_{13}H_{11}ClN_4O$) crystallizes in the monoclinic crystal system in the space group $P2_1/c$. The unit cell constants are: $a = 12.0965(7)$ Å, $b = 13.6075(7)$ Å,

Table 1. The crystal data and structure refinement details.

CCDC deposit No.	1838281
Shape, Color	Block, Yellow
Crystal size	$0.20 \times 0.15 \times 0.10\,mm^3$
Empirical formula	$C_{13}H_{11}ClN_4O$
Formula weight	274.71
Temperature	293 K
Radiation, Wavelength	MoK_α, 0.71073 Å
θ range for entire data collection	3.00° to 26.40°
Crystal system, Space group	Monoclinic, $P2_1/c$
Cell parameters	$a = 12.0965(7)$ Å $b = 13.6075(7)$ Å $c = 7.7686(4)$ Å $\beta = 93.942(3)°$
Volume	1275.71(12) $Å^3$
Z	4
Density (calculated)	1.430 Mg m^{-3}
Absorption coefficient	0.296 mm^{-1}
F_{000}	568
Index ranges	$-15 \leq h \leq 15$ $-17 \leq k \leq 17$ $-9 \leq l \leq 9$
Reflections collected	38427
Independent reflections	2606 [$R_{int} = 0.0569$]
Absorption correction	Multi-scan
Refinement method	Full matrix least-squares on F^2
Data / restraints / parameters	2606 / 0 / 174
Goodness-of-fit on F^2	1.110
R-sigma	0.0258
Final [$I > 2\sigma(I)$]	R1 = 0.0530, $wR_2 = 0.1416$
R indices (all data)	R1 = 0.0782, $wR_2 = 0.1686$
Extinction coefficient	0.040(7)
Largest diff. peak and hole	0.345 and -0.322 e$Å^{-3}$
Measurement	Bruker CMOS Diffractometer
Software for structure solution	SHELXS97
Software for refinement	SHELXL97
Software for molecular plotting	ORTEP PLATON Mercury

$c = 7.7686(4)$ Å and $\beta = 93.942(3)°$. The *ORTEP* of the compound is shown in Fig. 3a. The density functional theory (DFT) calculations for the compound were carried out with optimized [B3LYP/6-31 + G(d,p)] basis set using *Gamess* software program [23]. The optimized structure of the compound is shown in Fig. 3b. DFT calculations were performed in order to compare the theoretical values and the values obtained from XRD like bond lengths and bond angles. The calculated and experimental results are almost the same as shown in Table 2, and Fig. 4. Figure 4a illustrates the agreement between DFT and XRD bond lengths with correlation coefficient $R^2 = 0.9828$. Most of the calculated and experimental bonds lengths are nearly the same (Fig. 4b). Noticeable agreements between DFT and XRD bonds angles with $R^2 = 0.9902$ are also seen (Fig. 4c). In most cases, the calculated and experimental angles values are almost identical (Fig. 4d). A comparison of a few selected torsion angles from XRD and DFT are listed in Table 3.

The frontier molecular orbitals HOMO and LUMO of the compound were generated. HOMO means the highest occupied molecular orbital and LUMO refers to the lowest unoccupied molecular orbital. For the compound CMTP, the molecular orbital energies and their energy gaps were studied because the energy gap between the molecular

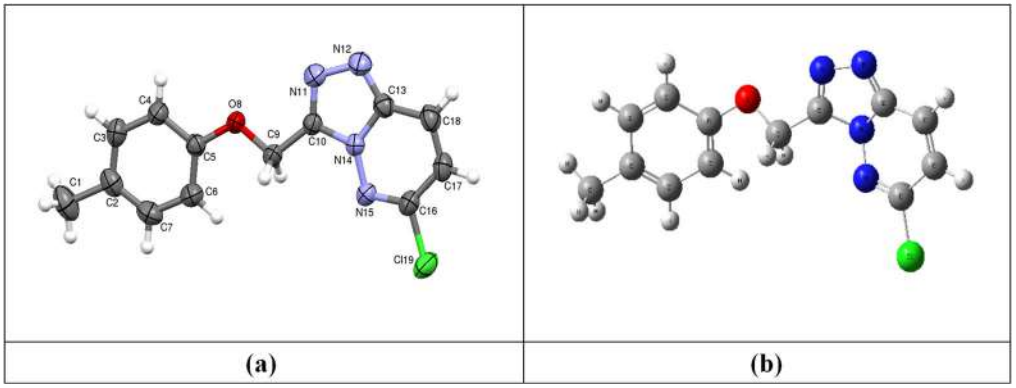

Figure 3. (a) The thermal ellipsoid plot of the compound with 50% probability ellipsoids. (b) DFT optimized structure of the compound CMTP.

orbitals often allows for a good description of the kinetic stability and chemical reactivity of the molecule. A molecule with a small energy gap between the molecular orbitals is more polarized, and is associated with low kinetic stability, high chemical reactivity, and is called a soft molecule. A large value of energy gap is generally associated with the high kinetic stability and low chemical reactivity [24]. The distribution of molecular orbitals HOMO and LUMO levels, and their energy gap for the compound are shown in Fig. 5. The HOMO and LUMO energies of the compound are −5.905 eV and −2.653 eV, respectively. The estimated energy gap between the HOMO and LUMO levels is 3.252 eV. The small HOMO-LUMO energy gap implies that the molecule is soft and more reactive. The HOMO is exactly localized in the phenoxy ring, oxygen atom, and methylene, whereas the LUMO is localized in triazole and pyridazine rings (nine membered ring C10/N14) and chlorine atom. Table 4 lists the energy gap and the other global reactivity descriptors including the ionization potential, the electron affinity, global hardness, global softness, the absolute electronegativity, the chemical potential, and the global electrophilicity for the compound.

3.2. Geometric structure

All the rings in the structure are in planar conformation. It is also evident by the torsion angles values for N12-N11-C10-C9 = −179.7(2)°, N11-N12-C13-C18 = −179.1(3)°, C13-N14-C10-C9 = 179.8(2)°, C10-N14-C13-N12 = 0.0(2)° and C3-C2-C7-C6 = −0.2(4)°. The maximum deviation from the plane for the five membered ring (C10-N11-N12-C13-N14) is 0.002(2) Å for N11; for the ring (C13-N14-N15-C16-C17-C18) is 0.009(2) Å for C16; for the ring (C2-C3-C4-C5-C6-C7) is 0.004(2) Å for C7; for the nine membered ring (C10-N11-N12-C13-C18-C17-C16-N15-N14) is 0.014(2) Å for N12. The triazole and phenoxy rings are bridged by C5-O8-C9-C10 group. This group is in plane with the triazole and phenoxy rings as indicated by the torsion angle values of 178.8(2)° for C5-O8-C9-C10 atoms. The methoxy-phenyl ring has nearly trigonal geometry as indicated by the bond angle values of C1-C2-C3 = 121.0(2)°, C1-C2-C7 = 122.0(2)°, C3-C2-C7 = 117.0(2)°, C3-C4-C5 = 119.8(2)°, C5-C6-C7 = 119.2(2)°, C2-C7-C6 = 122.8(2)°, C4-C5-C6 = 119.5(2)°.

Table 2. Comparison of bond lengths and bond angles.

No.	Bond (Å)		XRD	DFT	No.	Angle (°)				XRD	DFT
1	Cl19	C16	1.722	1.7446	**1**	C5	O8	C9	116.2		117.84
2	O8	C9	1.412	1.4087	**2**	N15	N14	C10	126.4		127.88
3	O8	C5	1.375	1.3745	**3**	N15	N14	C13	127.8		126.96
4	N14	N15	1.365	1.3564	**4**	C10	N14	C13	105.7		105.16
5	N14	C10	1.363	1.3682	**5**	N14	N15	C16	112.1		113.68
6	N14	C13	1.385	1.3972	**6**	N12	N11	C10	108.7		109.25
7	N15	C16	1.295	1.3034	**7**	N11	C10	N14	109.1		109.03
8	N11	C10	1.309	1.3230	**8**	N14	C10	C9	120.8		121.79
9	N11	N12	1.390	1.3690	**9**	N11	C10	C9	130.1		129.18
10	C10	C9	1.483	1.4978	**10**	O8	C9	C10	107.9		108.47
11	N12	C13	1.311	1.3234	**11**	N11	N12	C13	106.9		107.18
12	C17	C16	1.423	1.4360	**12**	C16	C17	C18	119.2		118.71
13	C17	C18	1.347	1.3694	**13**	O8	C5	C4	115.7		115.41
14	C5	C4	1.384	1.4027	**14**	O8	C5	C6	124.8		124.86
15	C5	C6	1.377	1.3975	**15**	C4	C5	C6	119.5		119.72
16	C4	C3	1.381	1.3906	**16**	C3	C4	C5	119.8		119.89
17	C13	C18	1.418	1.4158	**17**	N12	C13	N14	109.5		109.38
18	C6	C7	1.384	1.4026	**18**	N14	C13	C18	116.3		116.97
19	C3	C2	1.385	1.4073	**19**	N12	C13	C18	134.2		133.65
20	C7	C2	1.369	1.3970	**20**	Cl19	C16	N15	114.7		115.87
21	C2	C1	1.509	1.5126	**21**	Cl19	C16	C17	118.7		118.31
					22	N15	C16	C17	126.6		125.82
					23	C5	C6	C7	119.2		119.38
					24	C2	C3	C4	121.8		121.60
					25	C2	C7	C6	122.8		121.92
					26	C3	C2	C7	117.0		117.48
					27	C1	C2	C3	121.0		120.99
					28	C1	C2	C7	122.0		121.52
					29	C13	C18	C17	117.9		117.86

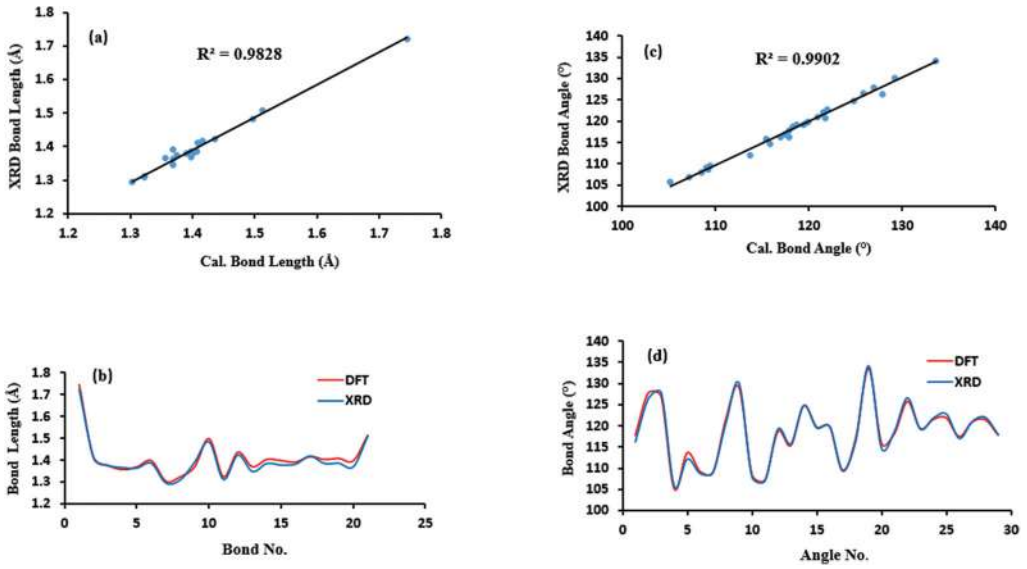

Figure 4. Plot of XRD versus DFT: (a) bond lengths (b) bond lengths vs. bond number. (c) bond angle values (d) bond angle values vs. angle number.

The structure is stabilized by C9-H9B … O8 and C17-H17 … N11 intermolecular hydrogen bond interactions given in Table 5. The crystal packing of the molecules viewed down *a* axis is shown in Fig. 6a. In the crystal, there is a molecule connected

Table 3. Selected torsion angles.

Atoms	XRD (°)	DFT (°)
C5-O8-C9-C10	178.8	−179.03
C10-N14-N15-C16	178.3	179.94
N15-N14-C10-N11	179.0	179.98
C13-N14-C10-N11	−0.2	−0.02
C4-C3-C2-C1	−179.4	−178.89
C18-C17-C16-CL19	179.2	−179.98
C10-N14-C13-N12	0.0	−0.01
O8-C5-C6-C7	−178.3	179.87
C3-C2-C7-C6	−0.2	−0.21
C13-N14-C10-C9	179.8	−179.71
N12-N11-C10-C9	−179.7	179.70

with two molecules, one through C9-H9B … O8 hydrogen bonds and another through C17-H17 … N11 hydrogen bonds. Furthermore, the hydrogen bonds in the structure exhibit $R_2^2(8)$ graph-set motif [25] which connects another two molecules in the crystal (see Fig. 6b). The crystal structure is reinforced by medium to weak π-π interactions (Table 6), as the centroid-centroid distance between the rings is less than 3.8 Å with small slip angles (β and $\gamma < 25°$). π-π stacking interactions occur between aromatic rings of the molecules due to their polarizable π electron densities which stabilizes the aromatic molecules. In Table 6, Cg1 is the centroid of the triazole ring, Cg2 is the centroid of the pyridazine ring, Cg3 is the centroid of the phenoxy ring, and Cg4 is the centroid of the nine membered ring.

3.3. Hirshfeld surface analysis

CrystalExplorer 17 [26] software was employed to study the Hirshfeld surface. 2D fingerprint plots were generated to find out the percentage contribution of each type of contact to the total Hirshfeld surface area. The Hirshfeld surface over normalized contact distance d_{norm} is shown in Fig. 7. This mapping uses red, blue, and white color schemes. The red and blue colored regions on the surface are from shorter and longer contacts than van der Waal's radii respectively; the white-colored regions are from contacts which are exactly equal to the van der Waal's radii [27]. The bright red region marked as **one** is from C9-H9B … O8 contact, **2** and **three** are from C17-H17 … N11 intermolecular hydrogen bonds.

The 2D fingerprint plots show the percentage contribution of each type of contact to the total Hirshfeld surface area. The strong intermolecular interactions appear as distinct spikes in the fingerprint plots. The decomposed fingerprint plots are shown in Fig. 8. Figure 8a presrnts all the contacts, and the shown green to blue-colored regions are from various π-π stacking interactions. Among all the contacts, the major contribution of 28.2% is from H-H contacts with $d_i + d_e \approx 2.4$ Å (Fig. 8b). O-H interactions appear as two characteristic spikes (Fig. 8f) and N-H interactions show two less distinct spikes (Fig. 8c), which have a significant contribution to the crystal packing where the distance $d_i + d_e \approx 2.35$ Å and 2.5 Å respectively. These interactions covering 5.2% and 20.2% to the Hirshfeld surface directly imply the greater effect of contribution by N-H rather compared to O-H. Cl-H and C-H contacts contribute 19.0% and 13.5% respectively to the Hirshfeld surface area.

The electrostatic potential mapped on Hirshfeld surface is generated using B3LYP function with 6-31G (d, p) basis set. In this map, we get a acurate picture of the

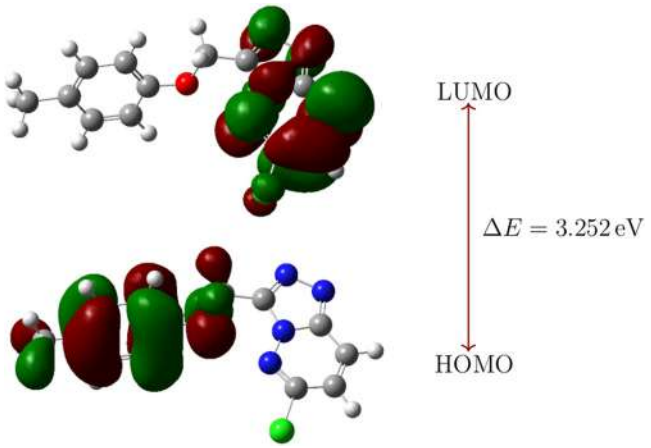

Figure 5. HOMO-LUMO and energy gap of the compound CMTP.

Table 4. HOMO-LUMO and Global reactivity descriptor values of the compound.

Parameters	Values
E_{HOMO} (eV)	−5.905
E_{LUMO} (eV)	−2.653
Energy gap (ΔE) (eV)	3.252
Ionization potential (I) (eV)	5.905
Electron affinity (A) (eV)	2.653
Chemical hardness () (eV)	1.626
Global softness (σ) (eV^{-1})	0.307
Eletronegativity (X) (eV)	4.279
Chemical potential (μ) (eV)	−4.279
Eletrophilicity (ω) (eV)	5.630

intermolecular interactions which are in charge of molecular packing in the crystal. The blue and red-colored regions on the electrostatic map represent the electropositive (hydrogen bond donor) and electronegative (hydrogen bond acceptor) respectively. On the electrostatic map, the electropositive region around C17-H17 atoms is complementary to the electronegative region near N11 atom (Fig. 9a). Curvedness is a function which is the root mean square curvature of the surface. It can be taken to recognize the particular planar arrangement and properties of packing modes [26]. Curvedeness plot mapped onto the surface shows the non-planar stacking between the molecules, since there is no flat surface seen on the curvedness plot (Fig. 9b).

Shape index gives direct insight into the stacking arrangement of molecules. Figure 9c displays the molecular Hirshfeld surface mapped over the shape index for the compound CMTP. Shape index maps are used to determine the concave region (red) and bumps (blue) where two molecular Hirshfeld surfaces touch each other [26]. The red colored-region on the shape index map represents the surface around the acceptor atoms, whereas the blue-colored region represents the surface around the donor atoms.

3.4. Energy frameworks

The calculations of the energy framework are based on B3LYP/6-31 G (d, p) functional basis set. The construction of energy frameworks gave a glance at the unique

Table 5. Hydrogen bonds geometry.

D-H … A	D-H (Å)	H … A (Å)	D … A (Å)	D-H … A (°)
C9–H9B … O8 [a]	0.97	2.50	3.439(3)	164
C17–H17 … N11[b]	0.93	2.56	3.260(3)	132

Note: symmetry codes [a] x,1/2-y,1/2 + z and [b] 1-x,1/2 + y,-1/2-z .

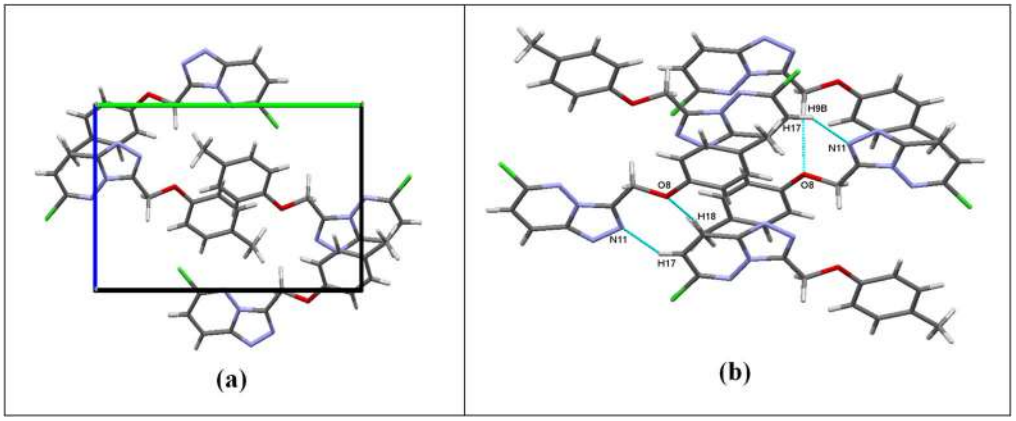

Figure 6. (a) The packing of the molecules viewed down *a* axis. (b) The packing diagram showing $R_2^2(8)$ graph-set motif involving C-H … O and C-H … N contacts.

Table 6. π-π interactions.

CgI	Cgj	Cg-Cg (Å)	α (°)	β (°)	γ (°)	CgI$_\perp$ (Å)	CgJ$_\perp$ (Å)	Slippage (Å)
Cg1	Cg2	3.5301(13)	1.37(12)	9.5	10.6	3.4696(9)	3.8421(9)	0.580
Cg1	Cg3	3.7065(14)	5.71(12)	20.3	24.9	3.3619(10)	−3.4754(10)	1.288
Cg1	Cg4	3.7641(12)	0.73(11)	22.0	22.7	−3.4775(9)	3.4902(9)	1.410
Cg2	Cg1	3.5301(13)	1.37(12)	10.6	9.5	3.4821(9)	3.4696(9)	0.650
Cg2	Cg4	3.5555(12)	0.65(9)	11.7	12.2	−3.4748(9)	3.4820(7)	0.719
Cg3	Cg1	3.7065(14)	5.71(12)	24.9	20.3	−3.4754(10)	3.3619(10)	1.561
Cg3	Cg4	3.6669(12)	6.42(9)	17.8	18.1	3.4853(10)	3.4923(7)	1.118
Cg4	Cg1	3.7640(12)	0.73(11)	22.7	22.0	3.4901(7)	−3.4725(9)	1.453
Cg4	Cg2	3.5555(12)	0.65(9)	12.2	11.7	3.4820(7)	−3.4748(9)	0.753
Cg4	Cg3	3.6670(12)	6.42(9)	18.1	17.8	3.4923(7)	3.4853(10)	1.140
Cg4	Cg4	3.4975(10)	0.02(7)	7.0	7.0	−3.4715(7)	−3.4715(7)	0.425

quantitative analysis of interaction energies. They have a predominant effect in the supramolecular architecture of molecules in the crystal [28, 29]. A cluster of molecules within a radius of 3.8 Å was generated around a single molecule. The interaction energies viz., electrostatic, polarization, dispersion, and repulsion, between the molecular pairs, were calculated (Table 7). R is the distance between molecular centroids (mean atomic position) in Å. The molecular pairs which are involved in the interaction along *b* axis are shown in Figure 10. The scale factors for benchmarked energies used for the construction of energy models were taken from Mackenzie et al. [29]. The visualization of different interaction energies coulomb interaction energy (red), dispersion energy (green), and total interaction energy (blue) of the compound along different axes are shown in Figure 11. The cylinders in the energy framework represent the relative strengths of molecular packing in several directions. In order to contract or expand the size of the cylinders in the framework, an overall scale factor is used [30]. The calculated interaction energies for electrostatic, polarization, dispersion and repulsion are −71.3 kJ/mol, −23.6 kJ/mol, −194.0 kJ/mol, and 117.0 kJ/mol

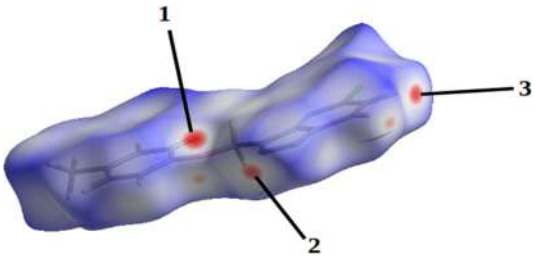

Figure 7. Hirshfeld surface mapped over d_{norm}.

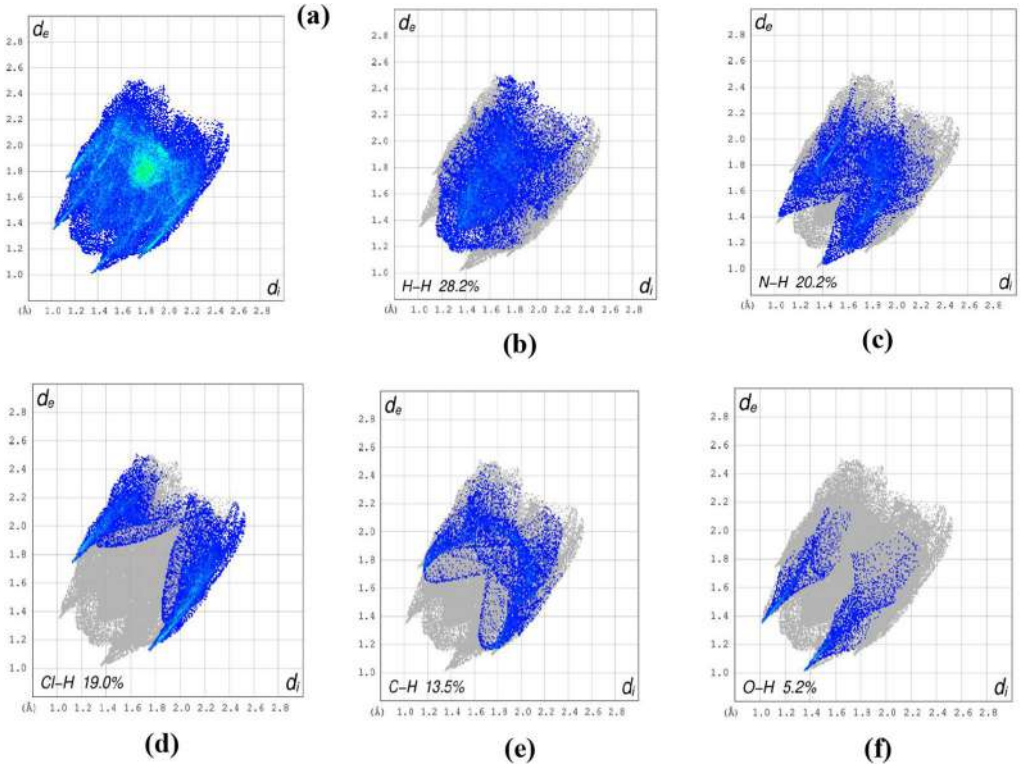

Figure 8. Fingerprint plots of the compound (a) From all the contacts (b) Decomposed fingerprint plot showing H-H (28.2%) contacts (c) N-H (20.2%) contacts (d) Cl-H (19.0%) contacts (e) C-H (13.5%) contacts (f) O-H (5.2%) contacts.

respectively. The total energy is −189.1 kJ/mol. The dispersion interaction energy dominates over the electrostatic Coulomb interaction energy. The scale factors used for the construction of energy framework for B3LYP/6-31G (d,p) electron densities are k_ele = 1.057, k_pol = 0.740, k_disp = 0.871, k_rep = 0.618 [28] (Figs. 10 and 11).

3.5. In vitro antioxidant activity

3.5.1. Free radical scavenging assay

Nitric oxide scavenging activity was measured by slightly modified methods of Marcocci et al. [31]. Nitric oxide radicals (NO) were generated from sodium nitroprusside. 1 mL

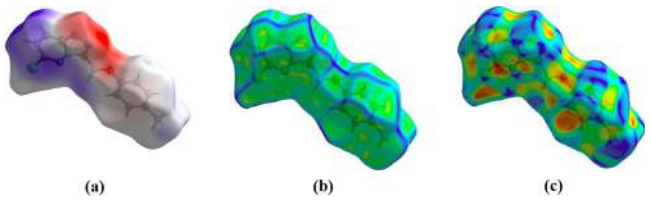

Figure 9. Hirshfeld surface (a) Electrostatic potential, (b) Curvedness and (c) Shape index map.

of sodium nitroprusside (10 mM) and 1.5 mL of phosphate buffer saline (0.2 M, pH 7.4) were added to different concentrations (25, 50, 75 and 100 mg/mL) of the test compounds, and incubated for 150 min at 25 °C and 1 mL of the reaction mixture was treated with 1 mL of Griess reagent (1% sulfanilamide, 2% H3PO4 and 0.1% naphthylethylenediamine dihydrochloride). The absorbance of the chromatophore was measured at 546 nm, and nitric oxide scavenging activity was calculated using the equation,

$$\% \text{ of scavenging} = [(A_{\text{control}} - A_{\text{sample}})/A_{\text{blank}}] \times 100.$$

Here, the antioxidant activity result shows that compound (CMTP) with chloro and methyl groups exhibit higher activity compared to standard drug.

	Concentration			
Compound	25	50	100	IC_{50}
CMTP	75.41 ± 0.17	87.60 ± 0.32	81.39 ± 0.60	17.01 ± 0.15
Ascorbic acid	88.49 ± 0.49	82.99 ± 0.19	83.61 ± 0.07	13.89 ± 0.54
Blank	–	–	–	–

(-) Shows no scavenging activity. Values are the means of three replicates ± SD.

3.6. Molecular docking studies on antioxidant

Prior to the simulations, bound ligand, cofactor, and water molecules were removed from the protein. The macromolecule was checked for polar hydrogen, and torsion bonds of the inhibitors were selected and defined. Gasteiger charges were computed, and the Auto Dock atom types were defined using Auto Dock version 4.2, the graphical user interface of Auto Dock supplied by MGL Tools [8, 32]. The binding free energy of a given inhibitor conformation in the macromolecular structure indicates how the small molecule, and the target macromolecule fit together. This can be useful for developing better drug candidates and also for understanding the nature of the binding. Molecular docking studies were carried out in order to explain in *silico* antioxidant studies, and a specific protein tyrosine kinase (1HD2) [33] was identified as the target for antioxidant compound. The molecular docking studies have been carried out to evaluate the binding of CMTP. The important binding interactions of the actively docked conformations of the ligand with the target proteins are identified one by one for all amino acids within 6 Å × 6 Å × 6 Å of the active site of the target protein. The binding interactions of the target compound have shown strong binding energy at −5.86 kJ/mol, compared to the standard drug that exhibited binding energy value of −4.89 kJ/mol as shown in Tables 8 and 9 and Figs. 12 and 13.

Table 7. Different interaction energies of the molecular pairs in kJ/mol.

N	Symmetry operation	R (Å)	Electron density	E_ele	E_pol	E_dis	E_rep	E_tot
2	x, -y+1/2, z+1/2	4.56	B3LYP/6-31G(d,p)	-13.6	-5.0	-59.6	37.9	-46.5
2	-x, y+1/2, -z+1/2	9.29	B3LYP/6-31G(d,p)	-28.2	-8.4	-19.6	21.5	-39.9
2	x, y, z	13.61	B3LYP/6-31G(d,p)	-2.1	-0.2	-6.0	5.3	-4.2
2	x, -y+1/2, z+1/2	11.88	B3LYP/6-31G(d,p)	1.1	-0.6	-7.0	4.0	-2.9
1	-x, -y, -z	6.98	B3LYP/6-31G(d,p)	-3.7	-4.5	-44.7	20.1	-33.7
1	-x, -y, -z	10.04	B3LYP/6-31G(d,p)	-18.2	-3.3	-9.0	3.6	-27.2
1	-x, -y, -z	11.37	B3LYP/6-31G(d,p)	-3.6	-1.1	-27.3	14.3	-19.5
1	-x, -y, -z	13.60	B3LYP/6-31G(d,p)	-0.6	-0.1	-7.8	2.6	-5.9
2	-x, y+1/2, -z+1/2	10.20	B3LYP/6-31G(d,p)	-2.4	-0.4	-13.0	7.7	-9.3

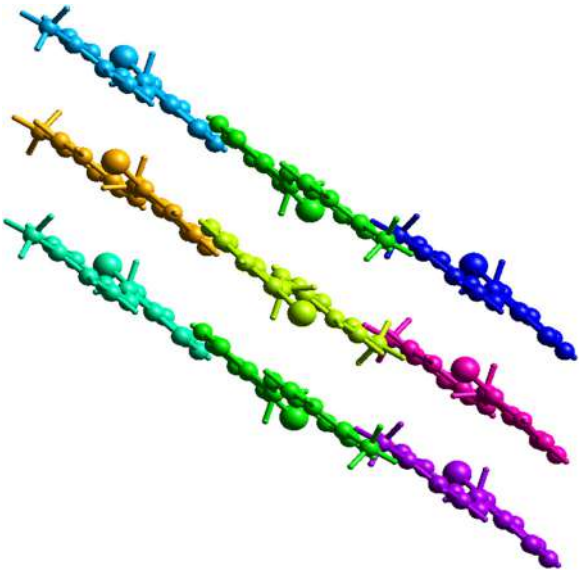

Figure 10. Molecular pairs involved in the calculation of interaction energies along *b* axis.

3.6.1. DNA interaction with CMTP is strong and attractive

Molecular docking studies of the compound CMTP with DNA duplex of sequence d(CGCGAATTCGCG)2 dodecamer (PDB ID: 1BNA) were performed, for the purpose of predicting the chosen binding site along with the preferred orientation of the molecules inside the DNA groove [34, 35]. From Table 10 and Fig. 14, it can be shown that the CMTP recognizes the narrow minor groove region of DNA groove mainly through phenoxy ring and situated within slim A-T regions due to the planarity of the molecule because of two aromatic phenoxy and pyridazine rings and preferential binding of A moiety to A-T regions which leads to van der Waals and hydrophobic interaction with DNA functional groups which stabilizes the groove and the complex. The complex

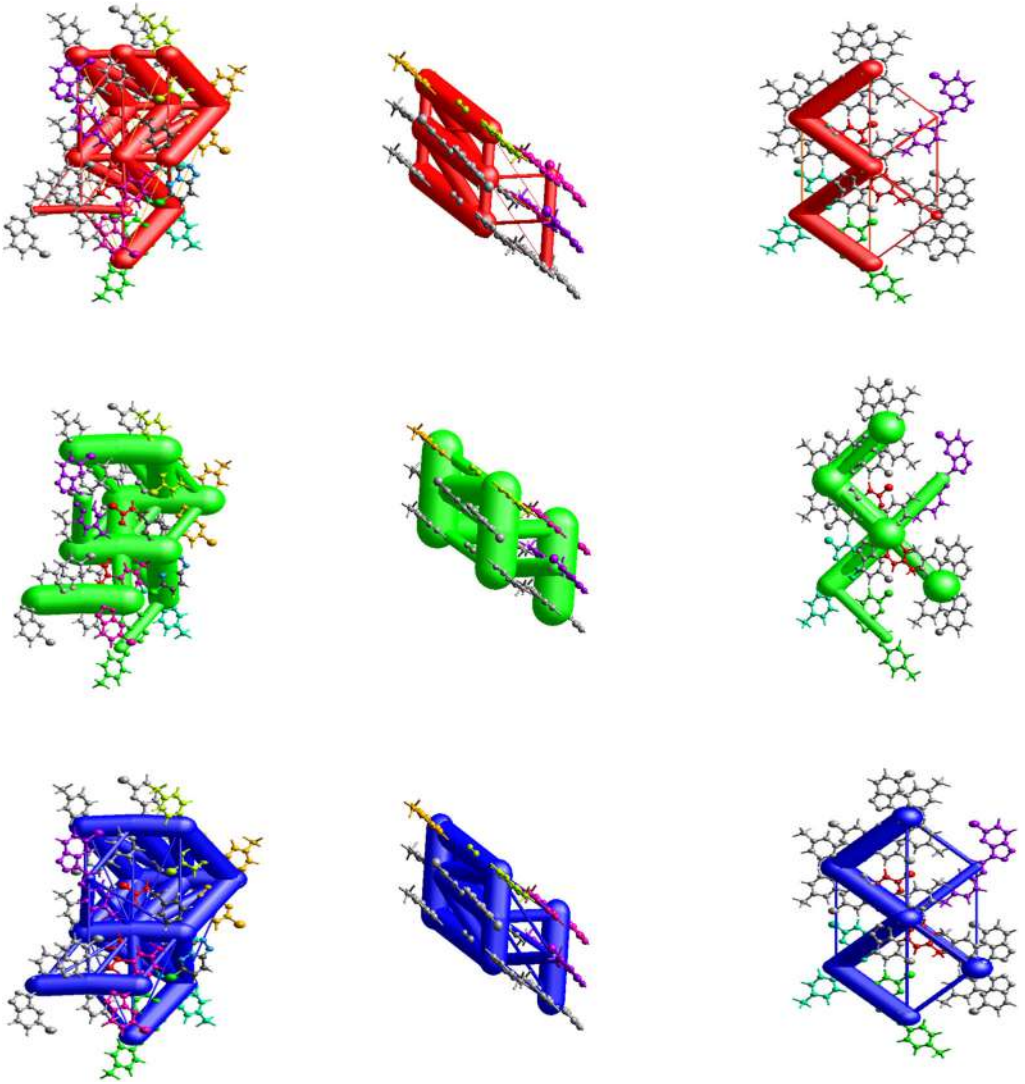

Figure 11. The graphical representation of electrostatic interactions: Coulomb interaction energy (red), dispersion energy (green), and total interaction energy (blue) of the CMTP along different axes.

shows the groove fit behavior and is arranged in a perpendicular manner with respect to the minor groove walls of the helix, and is stabilized by hydrogen bonding between the carbonyl group and hydroxyl groups of phenoxy ring as shown in Fig. 14. The binding energy of docked CMTP was found to be −6.35 kJ/mol (Table 10) which consequently determines the stable binding between DNA receptor and CMTP.

4. Conclusions

The compound CMTP ($C_{13}H_{11}ClN_4O$) crystallizes in the monoclinic crystal system. Hirshfeld surface analysis was performed in order to understand the intermolecular

Table 8. The dock score results of the **CMTP** with 1HD2 protein. (PDB code: 1HD2).

	mol	rseq	mseq	S	rmsd_refine	E_conf	E_place	E_score1	E_refine	E_score2
1		1	1	-5.8643	2.0128	11.1866	-46.5321	-9.0216	-30.8798	-5.8643
2	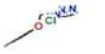	1	1	-5.8184	1.1173	11.1650	-50.2376	-9.3382	-30.6831	-5.8184
3		1	1	-5.3215	2.0691	12.1271	-55.7575	-8.9873	-25.4831	-5.3215
4	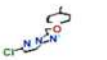	1	1	-5.2889	1.0470	12.1189	-48.7158	-8.6208	-24.5982	-5.2889
5	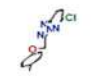	1	1	-5.1898	2.5917	11.6878	-47.4058	-9.5266	-22.1998	-5.1898

Table 9. The dock score results of the Ascorbic acid with 1HD2 protien. (PDB code: 1HD2).

	mol	rseq	mseq	S	rmsd_refine	E_conf	E_place	E_score1	E_refine	E_score2
1	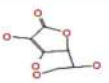	1	1	-4.8919	0.6332	91.9782	-81.4534	-10.2031	-25.1381	-4.8919
2	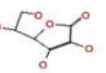	1	1	-4.7801	1.5062	89.8165	-77.0282	-10.8265	-25.0903	-4.7801
3	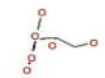	1	1	-4.7715	2.0723	85.0914	-94.7713	-10.1035	-22.5636	-4.7715
4	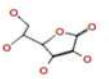	1	1	-4.7212	2.2425	86.3065	-70.6425	-10.3409	-24.4201	-4.7212
5		1	1	-4.7162	0.7605	86.9796	-70.8650	-10.4769	-24.0058	-4.7162

interactions. From the comparisons between the theoretical and experimental values, very good agreements are found between DFT and XRD values. The frontier molecular orbitals (HOMO-LUMO) and the energy gaps between them were calculated. The small energy gap (3.252 eV) between them indicates a soft molecule and easy transfer of

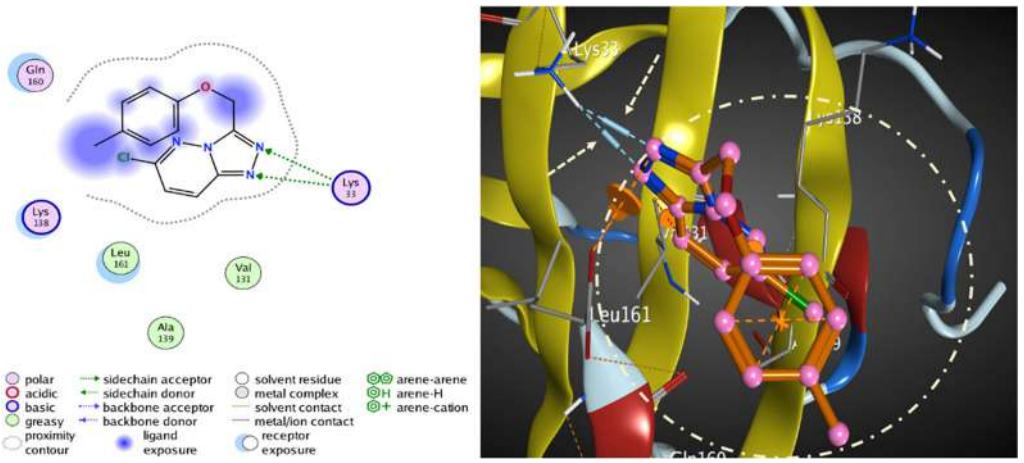

Figure 12. 3D and 2D interactions of compound CMTP with the 1HD2 protein by two hydrogen bonds with Lys 33 amino acid.

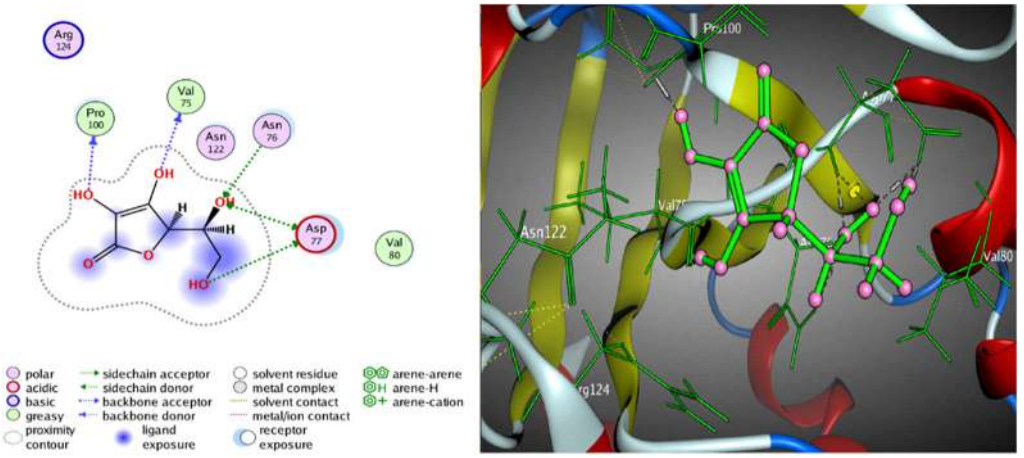

Figure 13. 3D and 2D interactions of the standard drug with the 1HD2 protein by two hydrogen bonds with Lys 33 amino acid.

electrons from HOMO to LUMO. An approach to comprehend the molecular packing in crystals via energy framework was accomplished. Different interaction energies, viz., electrostatic, dispersion, polarization, and repulsion between the molecular pairs were calculated. It was found out that the dispersion energy is the dominant factor. Results of the in *silico* study confirm that the compound CMTP is a promising high active molecule as antioxidant therapy and good binding energy with exact pocket side to the specific protein. It is evident that the interaction energy of the compound is lower compared to that of the standard, suggesting it to be selected as an antioxidant agent to the oxidative stress, caused by hydroxyl radicals. Molecular docking studies reveal that the compound exhibits high antioxidant activity compared to the standard drug.

Table 10. The dock score results of the the compound **CMTP** with DNA duplex of sequence d(CGCGAATTCGCG)2 dodecamer (PDB ID: 1BNA).

	mol	rseq	mseq	S	rmsd_refine	E_conf	E_place	E_score1	E_refine	E_score2
1		1	1	-6.3584	1.1812	11.3302	-39.7015	-9.3653	-34.7158	-6.3584
2		1	1	-6.1034	1.0591	10.8887	-49.6202	-8.6398	-36.7673	-6.1034
3		1	1	-6.0737	1.4486	12.4625	-47.2208	-8.8164	-29.4825	-6.0737
4	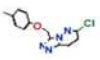	1	1	-6.0304	0.9461	11.9761	-43.7480	-9.0809	-37.2985	-6.0304
5	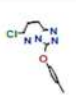	1	1	-5.9455	1.7565	11.3121	-55.8018	-8.9385	-35.1076	-5.9455

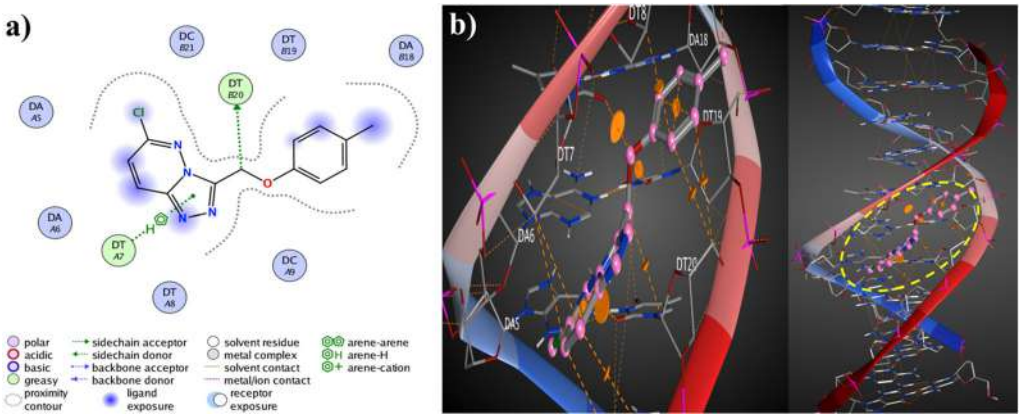

Figure 14. a) 2D interaction of DNA with the CMTP shows the sphere model of CMTP-DNA complex in the minor groove. b) 3D interaction of DNA with the CMTP shows the sphere model of CMTP-DNA complex in minor groove.

Author contributions

All authors have contributed in the preparation of the manuscript. Hamdi Hamid Sallam: Analysis and interpretation of the data, calculations, visualization, conceptualization, methodology, and writing-original draft. Yasser Hussien Eissa Mohammed and Fares Hezam Al-Ostoot: Synthesis, molecular docking studies, and writing chemistry draft. Geetha D.V.: Discussed the preparation of the manuscript and assistant in analysis of the data. Sridhar M. A.: Investigation, supervision, and approval of the final version.

Shaukath Ara Khanum: Synthesis, spectroscopic characterizations, and approval the chemistry draft.

Acknowledgments

Hamdi Hamid Sallam is thankful to Taiz University, Yemen, for providing financial assistance under the teacher's fellowship. Yasser Hussein Eissa Mohammed is thankful to the University of Hajjah, Yemen. Geetha thanks UGC BSR-RFSMS for providing fellowship. Fares Hezam Al-Ostoot is thankful to the government of Yemen and Al-Baydha University, Yemen, for providing financial assistance under the teacher's fellowship. Shaukath Ara Khanum thankfully acknowledges the financial support provided by VGST, Bangalore, under CISEE Program [Project sanction order: No. VGST/CISEE/282]. All the authors are grateful to the University of Mysore, Mysuru, India for providing laboratory facilities to carry out the research work and to SAIF, IIT Madras, for collecting single crystal X-ray diffraction data.

References

[1] K. Malinowsky *et al.*, *J. Cancer* **2**, 26 (2011). doi:10.7150/jca.2.26
[2] E. Vitaku, D. T. Smith, and J. T. Njardarson, *J. Med. Chem.* **57** (24), 10257 (2014). doi:10.1021/jm501100b
[3] H. H. Sallam *et al.*, *J. Mol. Struct.* **1237**, 130282 (2021). doi:10.1016/j.molstruc.2021.130282
[4] M. Asif, *Curr. Med. Chem.* **19** (18), 2984 (2012). doi:10.2174/092986712800672139
[5] N. O. Al-Harbi, S. A. Bahashwan, and K. A. Shadid, *J. Am. Sci.* **6** (7), 353 (2010).
[6] T. Akaberi, A. Shiri, and S. Sheikhi-Mohammareh, *J. Chem. Res.* **40** (1), 44 (2016). doi:10.3184/174751916X14497690510968
[7] A. A. Chavan, and N. R. Pai, *Molecules* **12** (11), 2467 (2007). doi:10.3390/12112467
[8] Y. H. E. Mohammed *et al.*, *Biomed. Pharmacother.* **95**, 375 (2017).
[9] E. Banoglu *et al.*, *Turk. J. Chem.* **31** (6), 677 (2007).
[10] E. M. Flefel *et al.*, *Molecules* **22** (1), 148 (2017). doi:10.3390/molecules22010148
[11] M. Tawfiq, *Int. J. Adv. Res.* **4**, 158 (2015).
[12] V. Pogacic *et al.*, *Cancer Res.* **67** (14), 6916 (2007). doi:10.1158/0008-5472.CAN-07-0320
[13] J. Xie, and J. Bai, *J. Cent. South Univ. (Med. Sci.)* **39** (7), 649 (2014).
[14] M. Y. Jaballah, R. T. Serya, and K. Abouzid, *Drug Res. (Stuttg.)* **67** (3), 138 (2017). doi:10.1055/s-0042-119992
[15] H. H. Sallam *et al.*, *J. Mol. Struct.* **1246**, 131242 (2021). doi:10.1016/j.molstruc.2021.131242
[16] D. V. Geetha *et al.*, *J. Mol. Struct.* **1178**, 384 (2019). doi:10.1016/j.molstruc.2018.10.016
[17] F. H. Al-Ostoot *et al.*, *J. Appl. Pharma. Sci.* **9** (07), 42 (2019).
[18] J. Druey, K. Meier, and K. Eichenberger, *HCA* **37** (1), 121 (1954). doi:10.1002/hlca.19540370115
[19] *Bruker* 2016. *APEX3 Crystallography Software Suite.*
[20] G. M. Sheldrick, *Acta Crystallogr. C., Cryst. Struct. Commun.* **71** (1), 3 (2015).
[21] A. L. Spek, *Acta Crystallogr. A.,: Found. Crystallogr.* **46** (s1), c34 (1990).
[22] C. F. Macrae *et al.*, *J. Appl. Crystallogr.* **41** (2), 466 (2008). doi:10.1107/S0021889807067908
[23] M. W. Schmidt *et al.*, *J. Comput. Chem.* **14** (11), 1347 (1993). doi:10.1002/jcc.540141112
[24] J. I. Aihara, *Theor. Chem. Acc.* **102** (1-6), 134 (1999).
[25] J. Bernstein *et al.*, *Angew. Chem. Int. Ed. Engl.* **34** (15), 1555 (1995). doi:10.1002/anie.199515551
[26] M. A. Spackman, and D. Jayatilaka, *Cryst. Eng. Comm.* **11** (1), 19 (2009). doi:10.1039/B818330A
[27] J. J. McKinnon, D. Jayatilaka, and M. A. Spackman, *Chem. Commun.* **37**, 3814 (2007).
[28] A. J. Edwards *et al.*, *Faraday Discuss.* **203**, 93 (2017). doi:10.1039/c7fd00072c

[29] C. F. Mackenzie *et al.*, *IUCrJ* **4** (Pt 5), 575 (2017). doi:10.1107/S205225251700848X
[30] M. J. Turner *et al.*, *Chem. Commun. (Camb.)* **51** (18), 3735 (2015). doi:10.1039/c4cc09074h
[31] Y. Kotaiah *et al.*, *Eur. J. Med. Chem.* **58**, 340 (2012). doi:10.1016/j.ejmech.2012.10.007
[32] Y. H. E. Mohammed, and S. A. Khanum, *Medchemcomm.* **9** (4), 639 (2018). doi:10.1039/c7md00593h
[33] N. Puttaswamy *et al.*, *Biomed. Pharmacother.* **103**, 1446 (2018). doi:10.1016/j.biopha.2018.04.167
[34] S. S. Mati *et al.*, *J. Phys. Chem. B.* **117** (47), 14655 (2013). doi:10.1021/jp4090553
[35] P. Pandya *et al.*, *J. Chem. Sci.* **122** (2), 247 (2010). doi:10.1007/s12039-010-0029-4